JACS
JOURNAL OF THE AMERICAN CHEMICAL SOCIETY

Article

pubs.acs.org/JACS

Mesoporous Aluminosilicate Catalysts for the Selective Isomerization of *n*-Hexane: The Roles of Surface Acidity and Platinum Metal

Nathan Musselwhite,[†,‡,∥] Kyungsu Na,[†,‡,§,∥] Kairat Sabyrov,[†,‡] Selim Alayoglu,*[,‡] and Gabor A. Somorjai*[,†,‡]

[†]Department of Chemistry, University of California at Berkeley, Berkeley, California 94720, United States
[‡]Chemical Sciences Division, Lawrence Berkeley National Laboratory, One Cyclotron Road, Berkeley, California 94720, United States
[§]Department of Chemistry, Chonnam National University, Gwangju, 500-757, South Korea

Supporting Information

ABSTRACT: Several types of mesoporous aluminosilicates were synthesized and evaluated in the catalytic isomerization of *n*-hexane, both with and without Pt nanoparticles loaded into the mesopores. The materials investigated included mesoporous MFI and BEA type zeolites, MCF-17 mesoporous silica, and an aluminum modified MCF-17. The acidity of the materials was investigated through pyridine adsorption and Fourier Transform-Infrared Spectroscopy (FT-IR). It was found that the strong Brönsted acid sites in the micropores of the zeolite catalysts facilitated the cracking of hexane. However, the medium strength acid sites on the Al modified MCF-17 mesoporous silica greatly enhanced the isomerization reaction. Through the loading of different amounts of Pt into the mesopores of the Al modified MCF-17, the relationship between the metal nanoparticles and acidic sites on the support was revealed.

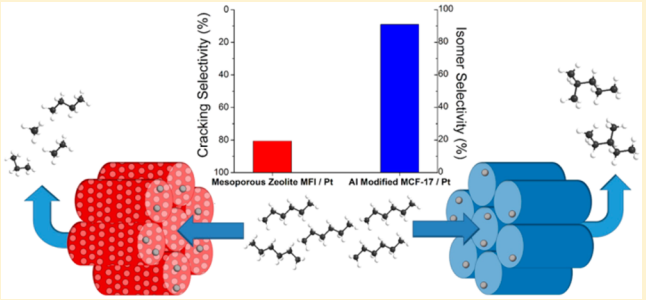

INTRODUCTION

The primary ambition of catalysis is to achieve optimal activity, while still retaining high selectivity to desired products.[1−3] By converting reactants into higher value products and eliminating undesired byproducts in an industrial reaction, the concept of green catalytic chemistry is realized.[4,5] Through careful investigation, understanding and control of the active sites of a catalyst, it is possible to tune reaction selectivity to accomplish these goals.[6−8]

One such important industrial reaction is the reforming of the naphtha feedstock of crude oil to make high octane gasoline. This process is typically run over platinum loaded onto an acidic support, such as acidified alumina or acidic aluminosilicates, such as zeolites.[9] Naphtha reforming is a multiproduct, multipath reaction with the goal to isomerize linear hydrocarbons into their branched counterparts, which have a higher octane number. The most common undesired byproduct of this reaction is the conversion of the reactant into shorter chain hydrocarbons, which is known as cracking. Cracked products are unable to be used as gasoline, and also the cracking reaction creates carbonaceous deposits on the surface (known as coke), which can deactivate the catalyst.

The isomerization of *n*-hexane is often used to study naphtha reforming.[10] Hexane reforming provides an excellent model compound to garner mechanistic and kinetic insight into this complicated industrial reaction. Figure 1 displays the possible products that can be distinguished in a typical hexane reforming reaction. The desired isomer products include the monobranched pentane multibranched butane species, cyclohexane, and methylcyclopentane. Undesired products include cracked C1−C5 hydrocarbons, dehydrogenated species, and benzene (which cannot be used in gasoline due to its carcinogenic properties).

Herein, we report on various aluminosilicate catalyst support materials for the reforming of *n*-hexane. We find that the catalyst which contains only mesopores and no micropores is capable of producing reaction selectivity leading to isomerization. We also correlate the acidity of each support material (determined through pyridine adsorption and FT-IR) to the catalytic selectivity of the support materials. The support which provides the best isomer selectivity contains no strong Brönsted acid sites and only medium strength Lewis sites. Therefore, the highest selectivity toward isomerization is achieved when platinum metal and mild Lewis acid sites work in tandem, without the solitary cracking chemistry of strong Brönsted acid sites in the zeolite micropores.

EXPERIMENTAL SECTION

Material Synthesis. We utilized previous reported literature procedures and practices for synthesizing all discussed materials.[11−15] Further synthesis details can be found in the Supporting Information. Two different mesoporous zeolites, with framework types BEA and MFI, mesoporous silica MCF-17, and Al modified MCF-17 were synthesized.

For mesoporous BEA zeolite, a cyclic diammonium-type organic molecule was used as the zeolite structure-directing agent (SDA), which was synthesized through an organic reaction following previous

Received: May 8, 2015
Published: July 13, 2015

DOI: 10.1021/jacs.5b04808
J. Am. Chem. Soc. 2015, 137, 10231−10237

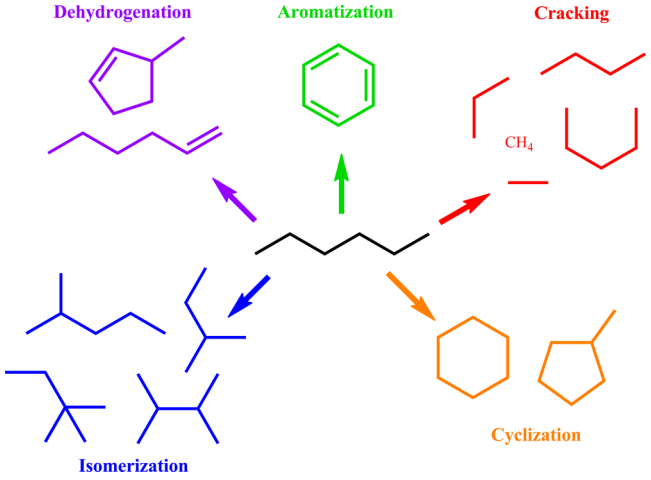

Figure 1. Scheme showing the possible products in the catalytic reforming of *n*-hexane. Isomerization and cyclization products are desired, while dehydrogenation, aromatization, and cracking are undesired. For all catalysts studied in this work, excluding unmodified MCF-17/Pt, isomer and cracking products accounted for over 98% of the total reaction products. The unmodified MCF-17/Pt catalyst also produced methylcyclopentane via cyclization.

literature.[11] In a typical zeolite synthesis, sodium-silicate was used as the silica source and $Al_2(SO_4)_3{\cdot}18H_2O$ was used as the alumina source. The silica and the alumina sources were dissolved in water with NaOH and organic SDA. After aging for 1 h at room temperature, the mixture was transferred to a Teflon-coated stainless-steel autoclave and heated at 170 °C for 1 d.

For mesoporous MFI zeolite, a diquaternary ammonium-containing organic surfactant was used as the zeolite SDA, which was synthesized via an organic reaction previously reported in the literature.[12] In a typical synthesis, sodium-silicate, $Al_2(SO_4)_3{\cdot}18H_2O$, NaOH, SDA, H_2SO_4, and distilled water were mixed to obtain a gel. The gel mixture was immediately shaken by hand very vigorously for 5 min to obtain as homogeneous a gel as possible. After further aging for 6 h under magnetic stirring in an oven at 60 °C, the gel was hydrothermally treated at 150 °C for 4 d.

MCF-17 type mesoporous silica was synthesized by previously reported literature methods.[13] Briefly, 1,3,5-trimethylbenzene (TMB), which was utilized as a pore swelling agent, was added to an aqueous solution of triblock copolymer Pluoronic P123 and HCl. After stirring of this solution for 2 h at 40 °C, tetraethylorthosilicate (TEOS) was added and the solution was stirred for an additional 20 h. NH_4F was then added, and the solution was allowed to hydrothermally react at 100 °C for 24 h. The product was then calcined for 6 h at 550 °C. The resultant zeolite precipitates and the mesoporous silica MCF-17 obtained after designated hydrothermal treatment times were collected by filtration, washed with distilled water, dried at 130 °C, and calcined at 550 °C for 4 h in air to remove organic species.

The mesopore surface of pure silica MCF-17 was aluminated through utilization of the grafting method.[15,16] The calcined sample was grafted with aluminum by slurring with anhydrous $AlCl_3$ in absolute ethanol, in order to give a Si/Al ratio of 8:1 or 36:1, as determined by inductively coupled plasma atomic emission spectroscopy (ICP-AES). The slurring solution was stirred overnight at room temperature, and then the ethanol was removed by rotary evaporation. The precipitated Al-modified MCF-17 was dried at 130 °C for 1 h and subsequently calcined at 550 °C for 4 h in air. All mesoporous materials (zeolites and Al-MCF-17) were further ion-exchanged to the H^+ form to introduce acidic functionality on the aluminosilicate framework.

Poly(vinylpyrrolidone) (PVP)-capped Pt nanoparticles (NPs) with an average size of 2.5 nm were synthesized by following the literature reported elsewhere.[17] In a typical synthesis, $H_2PtCl_6{\cdot}6H_2O$ was used as a Pt precursor, which was dissolved in ethylene glycol in the presence of PVP. This solution was reacted at boiling solvent temperatures, and the as-synthesized PVP-capped Pt NPs were washed and redispersed in ethanol to give a colloidal solution of Pt NPs with a concentration of 1 mg/mL. For supporting Pt NPs on porous supports, this colloidal solution of Pt NPs was added to the supporting materials to give the desired loading of Pt (~0.5 wt %). The colloidal suspension was sonicated for 5 h at room temperature using a commercial ultrasonic cleaner. The brown precipitates were separated by centrifugation, washed with ethanol, and dried in an oven at 60 °C overnight. All the prepared catalytic materials are summarized in Table 1. The two mesoporous zeolites without supporting Pt NPs were simply indicated as BEA and MFI, while the Pt NPs supported versions were indicated as BEA/Pt and MFI/Pt, respectively. The pure silica MCF-17 supporting Pt NPs was indicated as MCF-17/Pt, and the Al modified MCF-17 with Pt was indicated as Al-MCF-17/Pt.

Characterization. Transmission electron microscope (TEM) images of the zeolites, with and without Pt, were taken with a Hitachi H-7650 TEM operated at 120 kV. Postreaction characterization of the Al-MCF-17/Pt catalyst using scanning transmission electron microscopy (STEM)/energy dispersive spectroscopy (EDS) was conducted using a Jeol 2100F TEM. Point-to-point spatial resolution of the electron probe was 1.5 nm. Elemental analysis by ICP-AES was performed using a PerkinElmer optical emission spectrometer (Optima 7000 DV). N_2 physisorption analysis for determination of surface area and mesopore size was carried out using a Micromeritics ASAP2020 volumetric analyzer at the liquid nitrogen temperature (77 K). The surface area was calculated by Brunauer–Emmett–Teller (BET) equation from the adsorption data obtained at P/P_0 values between 0.05 and 0.2. The average mesopore size was determined from the adsorption branch of the isotherm using the Barrett–Joyner–Halenda (BJH) algorithm.

For IR measurement of mesoporous BEA and MFI zeolites, the H^+ form of the aluminosilicate samples were pressed to produce self-supporting wafers (ca. 12 mg/cm^2) without binding agents. The samples were subsequently degassed at 500 °C for 2 h in a lab-made in situ IR cell. After cooling down to room temperature, an organic base, pyridine, was used as a probe molecule. Pyridine was adsorbed on the acidic sites of the degassed samples at room temperature for 1 h. The physisorbed and weakly bound species were then desorbed for 1 h under vacuum at 150 °C. After cooling down to room temperature, IR spectra were collected using an FT-IR spectrometer (Nicolet Nexus-670) equipped with Mercury–Cadmium–Telluride (MCT) detector at room temperature with 80 scans and 2 cm^{-1} resolution for each spectrum. The concentration of Brönsted and Lewis acid sites was determined using a molar extinction coefficient (1.13 cm/μmol for Brönsted sites and

Table 1. Physicochemical Properties of Catalytic Materials

catalyst	Si/Al ratio	Pt loading[a] (wt %)	surface area (m^2/g)	mesopore size (nm)	micropore size (nm)	Brönsted acidity[b] (mmol/g)	Lewis acidity[b] (mmol/g)
BEA	8:1	0.5%	630	14	0.70	1.12	1.49
MFI	36:1	0.5%	610	11	0.55	0.13	0.25
MCF-17	no Al	0.5%	680	25	N/A	None	None
Al-MCF-17 (8)	8:1	0.5%	680	25	N/A	0.27	0.58
Al-MCF-17 (36)	36:1	0.5%	680	25	N/A	0.11	0.31

[a]All catalysts were evaluated with and without Pt NP loading. [b]Determined from integration of FT-IR data (see Figure 4).

DOI: 10.1021/jacs.5b04808
J. Am. Chem. Soc. 2015, 137, 10231–10237

1.28 cm/μmol for Lewis sites) of the pyridine IR band at 1550 $cm^{-1}$and 1450 cm^{-1}, respectively.[18]

Catalysis Studies. After synthesis, the catalytic behavior of the materials was investigated in the reforming of *n*-hexane. Catalytic measurements were made utilizing a tubular fixed catalyst bed reactor at ambient pressure, which has been described in previous publications.[10,15,19,20] Briefly, a 1/4 in. diameter stainless steel reactor was loaded with 0.2−0.5 g of catalyst (which was pelletized and sieved to yield 60−100 μm size granulates) and then capped on each end with a purified thermal silica filter. The remaining space in the reactor tube was filled with purified fused aluminum granulate and capped with glass wool. To keep the catalysis in a kinetic region and allow for selectivity comparisons, the total hexane conversion was held between 1% and 10%.

After loading, the catalysts were first pretreated at 633 K under a gas mixture of N_2 (Praxair, 5.0 UHP, 10 sccm) and H_2 (Praxair, 5.0 UHP, 10 sccm) for 2 h, with a heating rate of 2 K min^{-1}. After pretreatment, the reactor system was cooled to 513 K, under the same gas flow. The gas flow was then changed to 16 sccm H_2, and *n*-hexane (Fluka, ≥ 99.0%) was introduced using a Teledyne ISCO 500D liquid flow pump at a rate of 1.2 mL h^{-1} into the heated reactor head which was maintained at 423 K. In the reactor head, hexane was evaporated and mixed with H_2, resulting in a two-component gas flow with a hexane:H_2 ratio of 1:5 entering the reactor at near ambient pressure. A Baratron type (890B, MKS Instruments) manometer was used to monitor the reactor inlet pressure. The reaction products were sampled in the vapor phase at the reactor outlet and analyzed via an in-line gas chromatograph (GC), with all flow lines heated to 433 K. Quantitative analysis of product composition was accomplished with a Hewlett-Packard (5890 Series II) GC which was equipped with an Aldrich HP-1 capillary column and a flame ionization detector (FID). PC based GC Chemstation software (Hewlett-Packard) was utilized for automatic GC sampling, data collection, and postrun processing.

RESULTS AND DISCUSSION

The series of mesoporous aluminosilicate support materials investigated included (1) mesoporous zeolite type BEA, (2) mesoporous zeolite type MFI, and (3) mesoporous silica type MCF-17. The mesoporous silica MCF-17 support was also aluminated through a surface modification process with $AlCl_3$ in order to give identical Si:Al ratios to both the BEA (8:1) and the MFI (36:1) zeolites. All catalysts were investigated with and without 2.5 nm monodisperse Pt nanoparticles loaded into the mesopores of the material. A summary of all evaluated catalysts is shown in Table 1. Transmission Electron Microscope (TEM) images of the zeolite materials (with and without Pt nanoparticle loading) can be found in Figure S1. TEM and Scanning Transmission Electron Microscopy with Energy Dispersive Spectroscopy (STEM-EDS) images for the Al-MCF-17 loaded with Pt nanoparticles are shown in Figure S2.

The materials were investigated in the isomerization of *n*-hexane by using a tubular fixed bed reactor at ambient pressure. All reactions were run at 1−10%, in order to remain in the kinetic regime and to allow for selectivity comparisons. Further details about the flow reactor, catalytic test evaluations, and data processing can be found in the Supporting Information.

The catalytic performance of each support material was investigated both with and without Pt nanoparticles loaded into the mesoporous architecture. For all aluminosilicate catalysts, isomerization and cracking products accounted for over 98% of the total reaction products. Figure 2 presents mass activity for all studied catalysts. The two zeolite catalysts (BEA and MFI) showed high activity without the Pt, due to their catalytically active micropores. When Pt nanoparticles were loaded into the mesopores of the zeolites, the activity of the catalysts doubled and also the selectivity was improved. Figure 3 displays the isomer selectivity for BEA and MFI mesoporous zeolites with

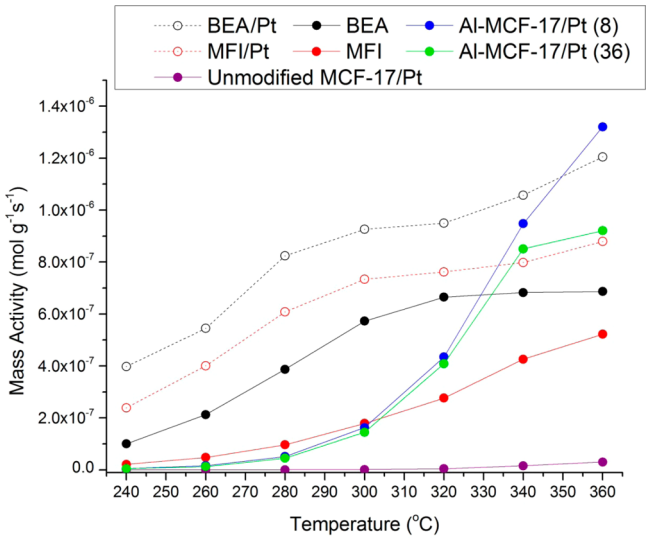

Figure 2. Mass activity (in terms of total moles of *n*-hexane converted per gram of catalyst per second) for all studied catalysts.

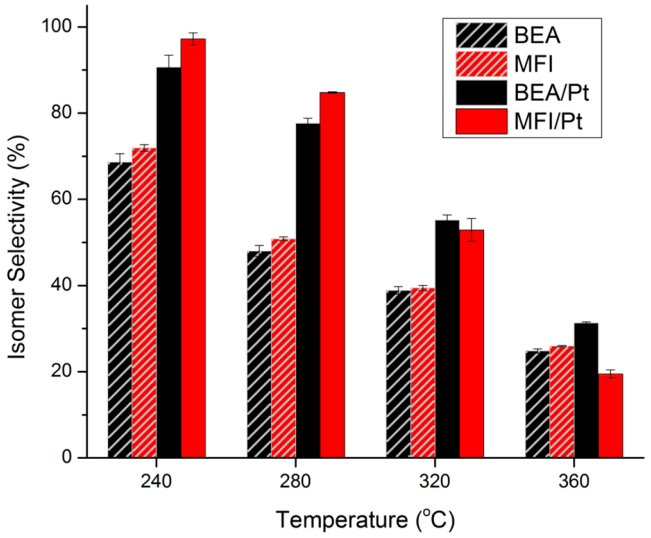

Figure 3. Total isomer selectivity of BEA (black/gray), MFI (red/gray), BEA/Pt (black), and MFI (red). It can be seen that at low temperatures the isomer selectivity is higher when Pt NPs are present in the mesopores of the zeolites. However, at higher temperatures the selectivity is nearly the same with or without Pt present, indicating the micropores of the zeolite dominate the catalytic chemistry. A more detailed plot with additional temperature points is shown in Figure S3.

and without Pt nanoparticles at various temperatures. A more detailed version of this plot can be found in Figure S3. It can be seen that the selectivity for isomerization is high at 240 °C, but drops to less than ∼25% on all zeolite catalysts at 360 °C, where the activity is highest (see Figure 3). Also of note is the fact that at lower temperature the Pt nanoparticle loading acts to increase the selectivity for isomers. However, at higher temperatures, the Pt loading has very little effect on selectivity for both zeolite catalysts. This suggests that at higher temperatures the micropores of the zeolite, which are excellent cracking catalysts, dominate the chemistry.[21−23]

All aluminum modified mesoporous silica materials (Al-MCF-17) were found to be inactive without Pt nanoparticles in the mesopores. However, when Pt nanoparticles were loaded into the mesoporous channels of the materials, the activity was comparable with the zeolite

DOI: 10.1021/jacs.5b04808
J. Am. Chem. Soc. 2015, 137, 10231−10237

catalysts (Figure 2). The selectivity and stability for these catalysts, however, were markedly improved compared to their zeolitic counterparts. The isomer selectivity for each catalyst is shown compared to the zeolite with the same Si:Al ratio in Figure 4, with a more detailed version shown that includes

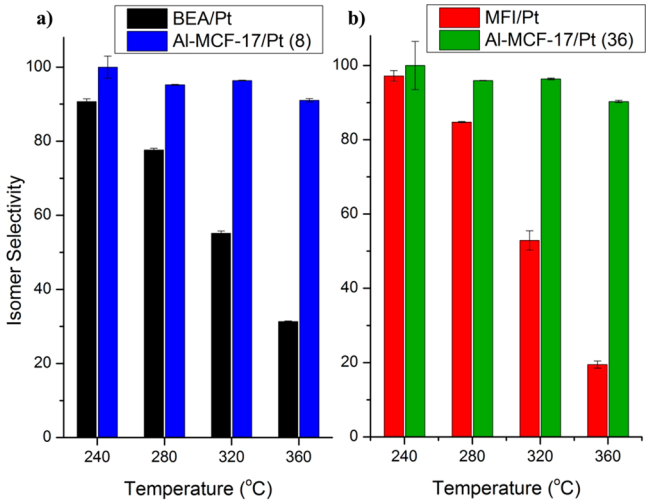

Figure 4. (a) Isomer selectivities for BEA/Pt zeolite (black) and Al-MCF-17/Pt (blue). Both catalysts shown contain a Si:Al ratio of 8:1. (b) Isomer selectivities for MFI/Pt (red) and Al-MCF-17/Pt (green). Both catalysts shown contain a Si:Al ratio of 36:1. In both plots the zeolite catalysts (BEA/Pt and MFI/Pt) drop in isomer selectivity as the reaction temperature increases. The Al modified MCF-17/Pt catalysts retain high isomer selectivity at higher temperatures. A more detailed version of this figure, with additional temperature points, is shown in Figure S5.

additional temperature points shown in Figure S4. The plot shows that as temperature increases, the zeolites isomer selectivity drastically decreases. However, the isomer selectivity of the Al modified catalysts remain high as temperature and subsequently overall activity increase. Furthermore, the stability of the mesoporous silica based catalysts is greater as compared to zeolite based catalysts. The mass activity at each temperature of the Pt loaded mesoporous zeolites significantly decreased after the first cycle, whereas the activity of the mesoporous silica based catalysts decreased only marginally as presented in Figure S5.

The unmodified MCF-17 selectivity is shown in Figure S6. When no Al modification is made to the MCF-17 mesoporous silica, the selectivity to overall isomers is only about 50%, and the activity is 2 orders of magnitude lower, as compared to the modified catalysts. Also, for the unmodified MCF-17/Pt catalyst, cyclization was also observed as an additional product, due to the ability of Pt metal to catalyze methylcyclopentane formation. This additional product was included into the total isomer product selectivity shown in Figure S6.

The strikingly higher isomer selectivity in the Al modified MCF-17 catalysts can be explained by two reasons: (1) the lack of catalytically active micropores on the Al-MCF-17 support material, which are known to activate the gas phase hexane directly and lead to cracking; and (2) the lack of strong Brönsted acidity on the surface of the Al-MCF-17 support, which are capable of cracking surface adsorbed hexane species. The well-accepted hexane isomerization mechanism proceeds via an adsorption/dehydrogenation on the Pt surface, followed by an isomerization on an acid site, and then subsequent desorption of the isomer.[24−29] However, when strong microporous acid sites exist, they are capable of activating the hexane without the presence of Pt.[30,31] This is evidenced by the activity of the mesoporous MFI and BEA zeolites without Pt. Strong Brönsted sites in zeolite micropores are known to lead primarily to cracked products at higher temperatures.[24,30,31] This agrees with the selectivity data shown in the plot in Figure 3. When Pt is added to the catalyst, the adsorption/dehydrogenation and subsequent isomerization cannot compete with the catalytic activity of the catalysis of micropores (as the number of Pt dehydrogenation sites is on average 2 orders of magnitude lower than the number of acid sites). The acid sites overwhelm the chemistry and the normal unimolecular isomerization mechanism is overwhelmed by a bimolecular mechanism, which leads to cracking products.[32] Therefore, at the higher temperature zone, where activity is optimized, it can be postulated that the strong Brönsted acidity of the zeolite micropores controls the chemistry, making cracking the dominant pathway.

In order to investigate the amount of acidic sites in the support materials, pyridine was used as a probe molecule and pyridine adsorption/desorption was studied with FT-IR. Experimental details are discussed in the Supporting Information. The spectra of all studied support materials are shown in Figure 5. All peaks were normalized to the Si−O−Si bond peak which ranges from 2100 to 1750 cm^{-1}. After normalization both Brönsted and Lewis acid sites are distinguishable at 1550 and 1450 cm^{-1}, respectively. Utilizing the adsorption coefficients of 1.13 cm/μmol for Brönsted sites and 1.28 cm/μmol for Lewis acid sites, the amount of each type of sites can be quantified by integration of the peaks.[33−35] The amount of each type of acid site is shown for each support material in Table 1.

Through the use of FT-IR we are able to quantify the amount and type of surface acid sites. In order to determine the relative strength of the acid sites we employ the same experiment with a temperature variant. If the acid site is stronger, it will retain the adsorbed pyridine at a higher temperature. Therefore, through integration of the FT-IR spectra we can infer the relative strength of the acid sites on each material based on the decrease in adsorbed pyridine with the increase in temperature.[35] These data are shown in Figure S7 and quantified in Figure 5b and 5c, of the manuscript. The plot in Figure 5b shows that MFI loses very little Brönsted adsorbed pyridine, even at high temperatures. This indicates that the catalyst contains a large amount of strong Brönsted acid sites. The BEA catalyst also retains some adsorbed pyridine at high temperatures. However, the two Al-MCF-17 catalysts drop to nearly zero as the temperature increases to 350 °C. This indicates that the Brönsted sites on the Al-MCF-17 supports are fairly weak, as compared to the zeolite catalysts. These findings about the Brönsted acidity of these materials agree with what Ryoo and co-workers determined for Al modified MCM-41 and mesoporous MFI zeolite using ^{31}P NMR characterization.[36] The presence of strong Brönsted acid sites leads to cracking in the hexane reforming reaction, due to the increased surface residence time and probability of β scission.[31,37,38]

The Lewis acid sites are shown in Figure 5c. The Al-MCF-17 supports and the BEA zeolite follow a similar trend of dropping to about 50% of the initial amount as the temperature increases. The MFI decreases slightly more than the other three materials, indicating it contains slightly weaker Lewis acid sites.

The main conclusion from these data is the retention of pyridine on the Brönsted acid sites of the zeolite catalysts, as compared to the Al-MCF-17 supports. If one assumes (1) that at 150 °C all Brönsted sites exist; (2) in the 150−250 °C range, weak Brönsted sites are released, so medium and strong Brönsted

DOI: 10.1021/jacs.5b04808
J. Am. Chem. Soc. 2015, 137, 10231−10237

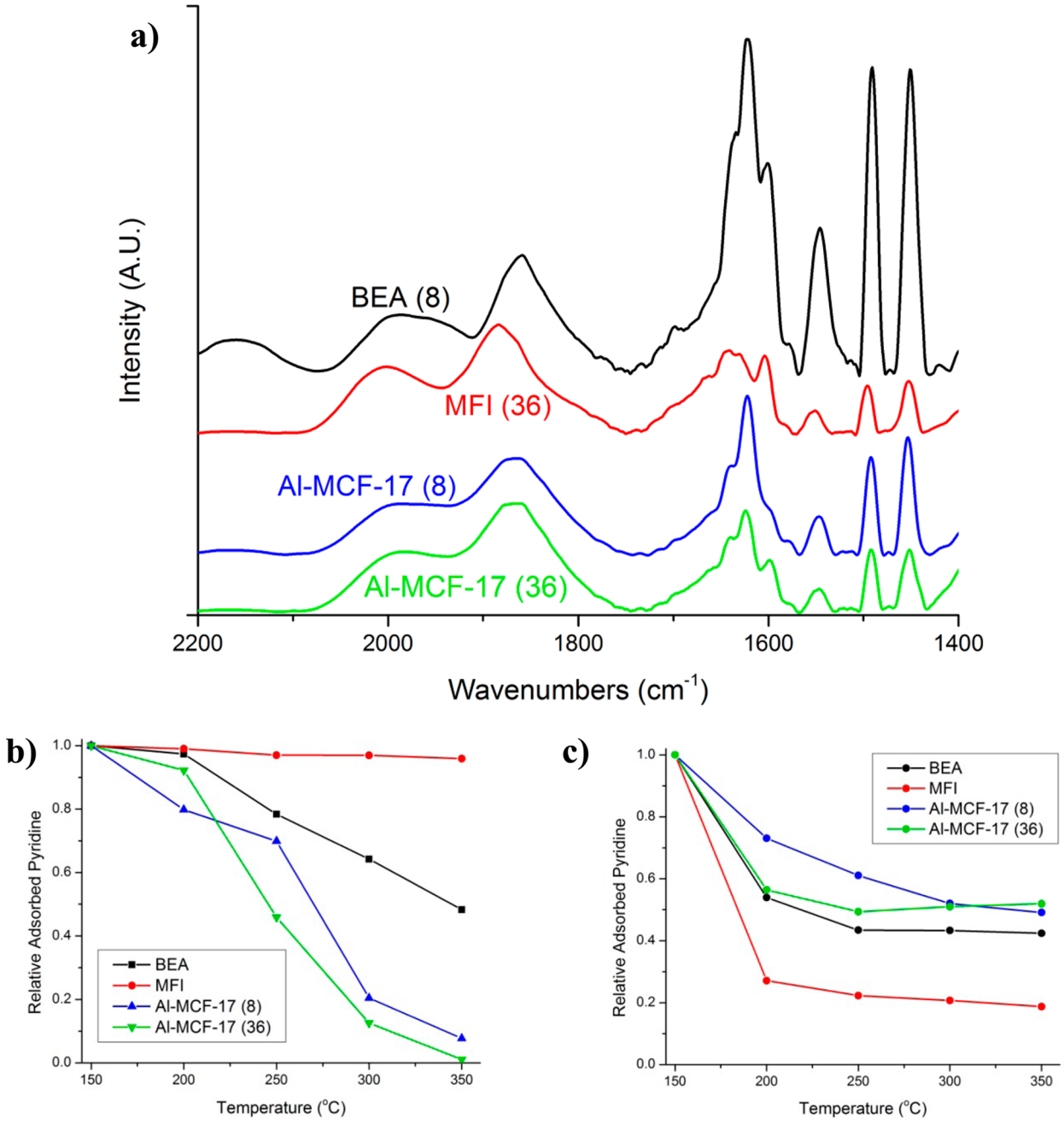

Figure 5. (a) FT-IR spectra of pyridine adsorbed onto mesoporous BEA (black), mesoporous MFI zeolite (red), aluminum modified MCF-17 with an 8:1 Si:Al ratio (blue), and aluminum modified MCF-17 with a 36:1 Si:Al ratio (green). The IR spectra are normalized with the band between 2100 and 1750 cm^{-1}, which originates from the Si−O−Si stretch. After pyridine adsorption, both Brönsted and Lewis acid sites are distinguishable at 1550 and 1450 cm^{-1}, respectively. Utilizing the adsorption coefficients of 1.13 cm/μmol for Brönsted sites and 1.28 cm/μmol for Lewis acid sites, the amount of each type of sites can be quantified (shown in Table 1). Si:Al ratios for each material are shown in parentheses. (b) The relative amount (normalized to initial spectrum at 150 °C) of Brönsted acid sites determined from FT-IR of adsorbed pyridine at 1550 cm^{-1} as a function of temperature. It can be seen that the amount of visible Brönsted sites on the MFI zeolite decreases very little with temperature, meaning the sites are relatively strong. The amount of pyridine adsorbed on Brönsted sites of the Al-MCF-17 support drops to nearly zero at higher temperatures, indicating that the sites are relatively weak. (c) The relative amount (normalized to initial spectrum at 150 °C) of Lewis acid sites determined from FT-IR of adsorbed pyridine at 1450 cm^{-1} as a function of temperature. The Al-MCF-17 and BEA catalysts appear to have medium strength Lewis sites, while the MFI zeolite contains slightly weaker Lewis sites.

sites are present; (3) and that at and above 350 °C only strong Brönsted sites remain, and the catalytic results can be elucidated. These findings suggest that the mesoporous zeolite catalysts contain strong Brönsted acid sites, which are capable of hexane activation without Pt, and also are selective toward cracking via the well-known β scission mechanism.[39,40] The Al-MCF-17 support contains relatively no strong Brönsted acid sites and accomplishes high isomerization selectivity via dehydrogenation on Pt and subsequent isomerization on medium strength Lewis sites and weak/medium strength Brönsted sites.[41]

The overall isomer production, or isomer yield, which is calculated from the product of the selectivity and activity at the

DOI: 10.1021/jacs.5b04808
J. Am. Chem. Soc. 2015, 137, 10231−10237

highest temperature studied (360 °C) is shown in Figure S8. This plot clearly shows that the Al-MCF-17/Pt catalysts are by far the best isomerization catalysts. However, the Al-MCF-17/Pt with the Si:Al ratio of 8:1 performs better than the 36:1 counterpart. From Figures 3 and S4, it can be seen that this difference comes not from a change in isomer selectivity, but from overall activity. To investigate this effect further, we loaded different amounts of Pt nanoparticles into the mesopores of the Al-MCF-17/Pt 8:1 catalyst in order to determine the effect of the ratio of Pt sites to acidic sites. These data are shown in Figure 6, and a more detailed

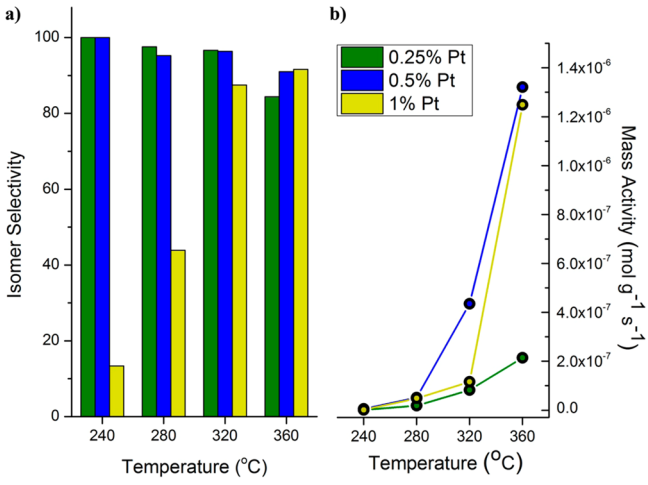

Figure 6. (a) Effect of Pt nanoparticle loading on the isomer selectivity and (b) the overall hexane conversion mass activity for the Al-MCF-17 (8) support material. It can be seen that when Pt loading is higher (1.0%, yellow), the selectivity at lower temperature suffers. When the loading is lower (0.25%, green), the catalyst loses activity. The optimal isomerization activity and selectivity are achieved with a 0.5% Pt loading on the Al-MCF-17 (8) support material (blue). More detailed versions of these plots, with additional temperature points, are shown in Figure S10.

version with additional temperature points is shown in Figure S9. It can be seen that when the Pt loading is 0.5% the catalytic activity and selectivity are maximized. When less Pt is loaded, the selectivity remains high, but activity is diminished. When more Pt is loaded, activity is high, but isomer selectivity at lower temperatures decreases. These effects are a result of varying the Pt site to acid site ratio, and not an effect of mass transport, which would only be seen for higher Pt loadings (above 1%).

To further explain these results, a calculation of the number of acid sites within an effective radius (r, where $2r$ is the distance between two nanoparticles). A scheme explaining this calculation is shown in Figure S10. The calculation shows that when Pt loading is too low, there are too many acid sites in the effective radius, and dehydrogenated surface adsorbed dehydrogenated "hexene" species are not adequately plentiful and overall turnover is low. If Pt loading is too high, the small amount of acid sites in the effective radius of the nanoparticle become overwhelmed with surface adsorbed species and selectivity is decreased because the Pt behaves as the catalyst without the acid sites, as in the unmodified MCF-17 shown in Figure 2. Therefore, in order to maximize selectivity and activity, a 0.5% Pt loading on a 8:1 Si:Al catalyst provides the perfect ratio of metal and acid sites.

CONCLUSIONS

In this work we have studied several types of aluminosilicate catalysts for the isomerization of *n*-hexane, both with and without Pt nanoparticles. We find that the best catalyst is Pt loaded onto an aluminum modified mesoporous silica (Al-MCF-17). The reason for this high isomer production is due to the mild Lewis acid and Brönsted acid sites that the aluminum modification supplies. This catalyst proved to be much more effective compared to the studied mesoporous zeolite catalysts, which were shown by FT-IR to contain strong Brönsted acid sites which were selective toward the undesired cracking products. We also find that, for the Al-MCF-17/Pt catalyst, the Pt loading plays a major role in the activity and selectivity of the reaction. If the loading is too low, activity suffers, because adsorbed intermediates cannot react quickly enough. If the loading is too high, metal catalysis becomes dominant and selectivity suffers. The optimum isomerization production occurs when Al-MCF-17, with a 8:1 Si:Al ratio, is loaded with 0.5 wt % Pt. The results in this manuscript demonstrate how, through careful synthetic control, the essential components for efficient catalysis can be determined, studied, and tailored to produce maximum catalytic efficiency.

ASSOCIATED CONTENT

Supporting Information

Details of the experimental procedure, figures presenting TEM images together with color-coded EDS spectral maps of the catalysts, plots presenting detailed reaction selectivity, activity, and stability of the catalysts, and FT-IR spectra of pyridine absorbed Al-MCF-17 and representation of radial density of acidic sites in Al-MCF-17/Pt. The Supporting Information is available free of charge on the ACS Publications website at DOI: 10.1021/jacs.5b04808.

AUTHOR INFORMATION

Corresponding Author

*somorjai@berkeley.edu
*salayoglu@lbl.gov

Notes

The authors declare no competing financial interest.

Author Contributions

‖N.M. and K.N. contributed equally.

ACKNOWLEDGMENTS

This work is funded by The Chevron Energy Technology Company. We acknowledge support from the Director, Office of Science, Office of Basic Energy Sciences, Division of Chemical Sciences, Geological and Biosciences of the U.S. DOE under Contract DE-AC02-05CH11231. K.N. thanks the Korea CCS R&D Center (KCRC) grant funded by the Korea government (Ministry of Science, ICT & Future Planning, NRF-2014M1A8A1049254). Work at the Molecular Foundry was supported by the Director, Office of Science, Office of Basic Energy Sciences, Division of Material Sciences and Engineering, of the U.S. Department of Energy under Contract No. DE-AC02-05CH11231.

REFERENCES

(1) Somorjai, G. A.; Li, Y. *Introduction to Surface Chemistry and Catalysis*; Wiley: New York, 2010.
(2) Somorjai, G. A.; Frei, H.; Park, J. Y. *J. Am. Chem. Soc.* **2009**, *131*, 16589−16605.
(3) Ertl, G.; Freund, H. J. *Phys. Today* **1999**, *52*, 32−38.
(4) Clark, J. H. *Green Chem.* **1999**, *1*, 1−8.
(5) An, K.; Alayoglu, S.; Musselwhite, N.; Na, K.; Somorjai, G. A. *J. Am. Chem. Soc.* **2014**, *136*, 6830.

DOI: 10.1021/jacs.5b04808
J. Am. Chem. Soc. 2015, 137, 10231−10237

(6) Campbell, C. T. *Surf. Sci. Rep.* **1997**, *27*, 1−111.
(7) Weckhuysen, B. M. *Chem. Commun.* **2002**, 97−101.
(8) Musselwhite, N.; Somorjai, G. A. *Top. Catal.* **2013**, *56*, 1277−1283.
(9) Antos, G. J., Aitani, A. M., Eds. In *Catalytic Naphtha Reforming*; CRC Press: New York, 2004.
(10) Musselwhite, N.; Alayoglu, S.; Melaet, G.; Pushkarev, V. V.; Lindeman, A. E.; An, K.; Somorjai, G. A. *Catal. Lett.* **2013**, *143*, 907−911.
(11) Na, K.; Choi, M.; Ryoo, R. *J. Mater. Chem.* **2009**, *19*, 6713−6719.
(12) Na, K.; Park, W.; Seo, Y.; Ryoo, R. *Chem. Mater.* **2011**, *23*, 1273−1279.
(13) Alayoglu, S.; Aliaga, C.; Sprung, C.; Somorjai, G. A. *Catal. Lett.* **2011**, *141*, 914−924.
(14) Jun, S.; Ryoo, R. *J. Catal.* **2000**, *195*, 237−243.
(15) Musselwhite, N.; Na, K.; Alayoglu, S.; Somorjai, G. A. *J. Am. Chem. Soc.* **2014**, *136*, 16661−16665.
(16) Jun, S.; Ryoo, R. *J. Catal.* **2000**, *195*, 237−243.
(17) An, K.; Alayoglu, S.; Musselwhite, N.; Plamthottam, S.; Melaet, G.; Lindeman, A. E.; Somorjai, G. A. *J. Am. Chem. Soc.* **2013**, *135*, 16689−16696.
(18) Triwahyono, S.; Jalil, A. A.; Ruslan, N. N.; Kamarudin, N. H. N. *J. Catal.* **2013**, *303*, 50−59.
(19) Pushkarev, V. V.; An, K.; Alayoglu, S.; Beaumont, S. K.; Somorjai, G. A. *J. Catal.* **2012**, *292*, 64−72.
(20) Pushkarev, V. V.; Musselwhite, N.; An, K.; Alayoglu, S.; Somorjai, G. A. *Nano Lett.* **2012**, *12*, 5196−5201.
(21) Bhan, A.; Gounder, R.; Macht, J.; Iglesia, E. *J. Catal.* **2008**, *253*, 221−224.
(22) Boronat, M.; Viruela, P.; Corma, A. *J. Phys. Chem. A* **1998**, *102*, 982−989.
(23) Chen, K.; Damron, J.; Pearson, C.; Resasco, D.; Zhang, L.; White, J. L. *ACS Catal.* **2014**, *4*, 3039−3044.
(24) Ciapetta, F. G.; Hunter, J. *Ind. Eng. Chem.* **1953**, *45*, 147−155.
(25) Barron, Y.; Maire, G.; Muller, J. M.; Gault, F. G. *J. Catal.* **1966**, *5*, 428−445.
(26) Konno, H.; Okamura, T.; Kawahara, T.; Nakasaka, Y.; Tago, T.; Masuda, T. *Chem. Eng. J.* **2012**, *207-208*, 490−496.
(27) Davis, R. J.; Derouane, E. G. *Nature* **1991**, *349*, 313−315.
(28) Davis, S. M.; Zaera, F.; Somorjai, G. A. *J. Am. Chem. Soc.* **1982**, *104*, 7453−7461.
(29) Davis, S. M.; Zaera, F.; Somorjai, G. A. *J. Catal.* **1984**, *85*, 206−223.
(30) Guo, Y. H.; Pu, M.; Wu, J. Y.; Zhang, J. Y.; Chen, B. H. *Appl. Surf. Sci.* **2007**, *254*, 604−609.
(31) Corma, A.; Orchilles, A. V. *Microporous Mesoporous Mater.* **2000**, *35-36*, 21−30.
(32) Blomsma, E.; Martens, J. A.; Jacobs, P. A. *J. Catal.* **1996**, *159*, 323−331.
(33) Guisnet, M.; Ayrault, P.; Coutanceau, M.; Fernanda Alvarez, M.; Datka, J. *J. Chem. Soc., Faraday Trans.* **1997**, *93*, 1661−1665.
(34) Ayrault, P.; Datka, J.; Laforge, S.; Martin, D.; Guisnet, M. *J. Phys. Chem. B* **2004**, *108*, 13755−13763.
(35) Barzetti, T.; Selli, E.; Moscotti, D.; Forni, L. *J. Chem. Soc., Faraday Trans.* **1996**, *92*, 1401−1407.
(36) Seo, Y.; Cho, K.; Jung, Y.; Ryoo, R. *ACS Catal.* **2013**, *3*, 713−720.
(37) Corma, A.; Planelles, J.; Sanchez-Marin, J.; Tomas, F. *J. Catal.* **1985**, *93*, 30−37.
(38) Feng, R.; Liu, S.; Bai, P.; Qiao, K.; Wang, Y.; Al-Megren, H. A.; Rood, M. J.; Yan, Z. *J. Phys. Chem. C* **2014**, *118*, 6226−6234.
(39) Yaluris, G.; Madon, R. J.; Dumesic, J. A. *J. Catal.* **1997**, *165*, 205−220.
(40) Li, Q.; East, A. L. L. *Can. J. Chem.* **2005**, *83*, 1146−1157.
(41) Li, Q.; Hunter, K. C.; East, A. L. L. *J. Phys. Chem. A* **2005**, *109*, 6223−6231.

DOI: 10.1021/jacs.5b04808
J. Am. Chem. Soc. 2015, 137, 10231−10237